Novel polyhedral mechanical metamaterial exhibiting negative Poisson's ratio

OPEN ACCESS
IOP Publishing
Smart Materials and Structures
Smart Mater. Struct. **32** (2023) 035008 (18pp)
https://doi.org/10.1088/1361-665X/acb3a3

Novel polyhedral mechanical metamaterial exhibiting negative Poisson's ratio

A Sorrentino* and **D Castagnetti**

Dipartimento di Scienze e Metodi dell'Ingegneria, Università di Modena and Reggio Emilia, Via G. Amendola 2, 42122 Reggio Emilia, Italy

E-mail: andrea.sorrentino@unimore.it

Received 16 November 2022, revised 8 January 2023
Accepted for publication 15 January 2023
Published 1 February 2023

Abstract

The work presents a novel polyhedral mechanical metamaterial based on rotating triangular prisms connected by their corners, which possesses the ability to attain large values of negative Poisson's ratio (NPR). Through a kinematic model of the proposed rotating structure, we evaluate the auxeticity of the system by varying the geometrical parameters of the polyhedrons composing the elementary cell of the structure. The kinematic results highlight the peculiar NPR of the system, whose values are nearly constant over significant strain ranges. Focusing on the most promising auxetic mechanisms we designed chiral architectures that replace the ideal hinges at the corners with curved-shape ligaments, and validated these configurations through three-dimensional printed specimens. The specimens were tested under uniaxial compression and simulated through finite element analyses. Experimental results exhibited an excellent agreement with computational predictions in terms of elastic modulus and auxeticity, showing a value of Poisson's ratio up to -1.3 for one of the designs. Our findings demonstrate the highly auxetic property of rotating polyhedral systems, which allow the design of novel architected materials useful, for example, in biomechanical applications.

Keywords: auxetic mechanical metamaterials, negative Poisson's ratio, rotating polyhedrons, hinged structures, additive manufacturing, experimental validation, finite element simulations

(Some figures may appear in colour only in the online journal)

1. Introduction

Mechanical metamaterials are artificial materials and structures for which mechanical performance are primarily influenced by their small-scale architecture and topological features [1–3]. As a result, these structures exhibit extreme mechanical and physical properties that gives rise to the desired macro-scale elastic properties, which are not commonly found in natural materials [4, 5]. Some of these materials possess the extraordinary property of negative Poisson's ratio (NPR), defined as auxetic metamaterials [6–10], whereby these structures contract in the transverse direction in response to a compression and vice-versa [11, 12]. This 'negative' behavior in auxetic metamaterials also promotes enhanced mechanical properties such as increased shear modulus [13] and indentation resistance [14, 15], synclastic curvature [16] and higher energy absorption capabilities [17], with applications in acoustic, electronics, biomechanics, textiles and personal protections [18–23]. The NPR in auxetic metamaterials governs the deformation behavior of these systems, and consequently, the toughness and strain capabilities of such mechanisms, which originates from their geometrical motif rather than their material composition [24]. Hence, auxeticity is a scale-independent property. According to literature, auxetic mechanical metamaterials comprise 2D structures such as

* Author to whom any correspondence should be addressed.

honeycombs, origami and membranes, and three-dimensional (3D) solids including foams and lattices, whose specific architecture allows to obtain a NPR [25–27]. Auxetic structures consist of deformation mechanisms like ribs/ligaments hinging, stretching or bending, and rotating [28, 29]. In particular, structures involving rotating (semi-) rigid units were extensively studied in the recent years [30].

Rotating auxetic mechanisms, referred to as hinged structures, consist of rigid units connected by hinges, which are arranged according to a consistent rule. Typical example of 2D motif is the rotating squares mechanism which possesses a Poisson's ratio equal to -1 [31]. Rigid unit motifs are not restricted to regular squares: also rectangles, triangles, rhombi, parallelogram cells, irregular shape units [32–34] and rotating cells with chiral ligaments [35, 36] can be retrieved from the literature. By analogy, 3D rotating structures can be designed using the structural motif of a 2D rotating unit structure, resulting in 3D polyhedral metamaterials able to generate auxetic effect. In this sense, earliest works explore the auxetic potential of tetrahedral frameworks in order to understand the NPR response observed in inorganic crystalline materials [37]. Hence, promising auxetic structures include rotating cuboidal units [38] and 3D cells based on chirality [39]. However, a structure made of cubes connected by pivots at their corners possess the potential to exhibits large values of NPR in all three directions [40]. Additionally, chiral-rotating units were designed and fabricated using additive manufacturing (AM) techniques, thus leading anisotropic lattice structures with a high value of NPR [35]. On the whole, structures with regular n-gonal polygonal prism-shaped unit cells demonstrate the ability to lead auxetic behavior [41]. Then, new types of 3D rotating auxetic geometries were recently proposed in literature [42–44].

This work proposes, develops and validates a novel polyhedral mechanical metamaterial with NPR, which consists of rigid triangular prism units connected by the corners. There are three main steps of this work: kinematic simulation, experimental validation and numerical analysis. The kinematic investigations focused on different configurations of the hinged structure and evaluate the auxeticity of the metamaterial. Hence, physical models were additively manufactured and experimentally validated. These consist of unit cells with curved-shape ligaments between the solid prims, thus obtaining a metamaterial with a Poisson's ratio up to -1.3. Using finite element (FE) models, we also assessed the mechanical properties of the proposed architected structure with ligaments, revealing a good correlation with the experimental results.

The work illustrates the tendency of NPR behavior of such metamaterials upon the variation of their geometrical parameters with the possibility to design novel auxetic architectures. Thanks to the tunable mechanical properties and functionalities of these metamaterials, a possible application is in the field of biomechanics, to design prostheses with an elastic response similar to that of human trabecular bones.

2. Auxetic polyhedral structure

The work concerns the development of a novel 3D auxetic structure containing rotating rigid polyhedral units. As shown in figure 1(A), the design of this metamaterial starts from a regular tessellation of the 2D space with equilateral triangles, where l is the side length of the polygons [45–47]. From this tiling, we identified four triangles which were used to construct the unit cell of the proposed architecture (see figure 1(A)). To attain the structure capable of undergoing deformation process potentially leading some exotic extreme negative mechanical properties, we modified the geometrical architecture in figure 1(A) by rotating the triangles by the internal angle θ, thus introducing voids in the structure. This leads to the architecture shown in figure 1(B), which features two axes of symmetry along the x- and y-directions, corresponding to the well-known triangle-based metamaterial configuration retrieved from the literature [48, 49]. Hence, we extruded the regular triangles composing the motif in figure 1(B) in the out-of-plane (y-direction), and mirroring them about the xz plane, thus obtaining eight triangular prisms with height, h (see figure 1(C)), that constitute the representative unit cell (RUC) of the proposed metamaterial when fully compressed (i.e. when closed), see figure 1(C). Specifically, we assumed that each prism of the system is connected to the adjacent polyhedral units by hinges at their vertices, highlighted as small circles in figure 1(C). Thus, by rotating the rigid units around their vertices (i.e. the pivoted corners), we improve the overall volume of the system and obtain voids in the metamaterial [50]. This tilting of the polyhedral elements leads to the final configuration in figure 1(D), where φ represents the characteristic angle of the polyhedral architecture. By repeatedly stacking up RUCs, we obtain a 3D polyhedral structure, which features a cubic symmetry with respect to the principal directions (see figures 1(C) and (D)). This architecture will clearly exhibit a NPR response, i.e. an auxetic behavior, when deformed along its principal directions (x, y, z), since pulling or compressing the nodes on two opposite faces will originate a transverse expansion or compression, respectively. The next section will investigate through quantitative kinematic analysis the effect of geometric parameters on the auxetic response of the structure.

3. Material and methods

3.1. Kinematic analysis of the hinged structure

Since the tilting of the unit cell in the system is determined by the combination of the three angles between the adjacent prisms in the corresponding principal directions, we evaluated the auxetic behavior of the polyhedral metamaterial by implementing a kinematic model of the structure using the CAD/CAE software *Solidworks* [51]. In particular, the model describes the prisms as rigid bodies and the hinges at their vertices as ideal (i.e. frictionless) [40]. Hence, the analyses

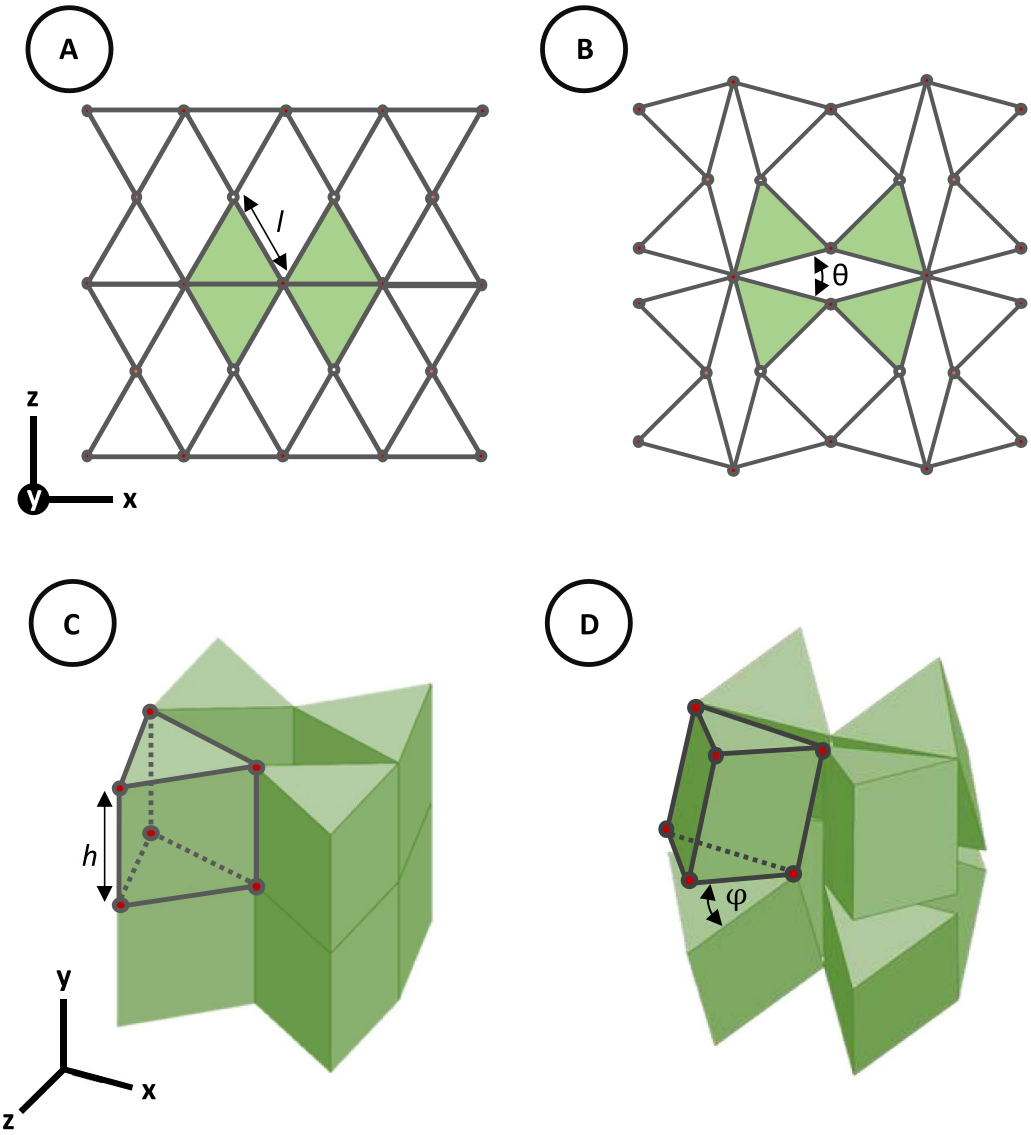

Figure 1. Geometric evolution steps of the proposed architected material: (A) initial tasseled two-dimensional space, (B) 2D geometrical representation of the RUC structure [48, 49], (C) RUC of the 3D architected structure when fully compressed (closed) and (D) stretched (open) unit cell configuration of the metamaterial.

applied periodic boundary conditions (PBCs) to the RUC of the structure (figure 2), which implies the simulation of the structure as an infinite system [52].

Periodicity of the RUC entails that all pairs of opposite boundary surfaces deform identically (front-back, top-bottom and right-left paired surfaces in figure 2). Specifically, we tied the vertices of an edge (surface) with the corresponding vertices on opposite edge. This enforces the same displacements in *x, y, z*-directions, respectively, for all the paired vertices of corresponding surfaces (the vertices on the boundary surfaces with the same color in figure 2). Additionally, the internal vertices of the prisms were coupled with the adjacent vertices of the attached rotating prims (i.e. the red dots in figure 2), in such way that hinge constraints connect the polyhedrons at these corners.

The peculiar deformation behavior of the metamaterial is strictly correlated to the internal angle θ of the system (see figure 1(B)), thus leading to different geometrical configurations of the structure when it is initially compressed along the *y*-axis. According to preliminary analyses of the structure, the internal angle of the system, i.e. θ, must be greater than 15°, to avoid any contact between the prisms at the beginning of the rotation. Symmetrically, since the polygons of the planar motif of the metamaterial are equilateral triangles, the θ angle must be lower than 75°.

To investigate the auxeticity of the proposed metamaterial, we performed a numerical analysis plan involving the following design variables. Firstly, the angle θ from 15° to 75° in steps of 15°, secondly, the height of the prism, *h*, over three levels (1, 1.25 and 1.5 mm), see figure 1. For all the simulated systems, we set the side length, *l*, of the polygons equal to 1 mm (see figure 1(A)), and, for simplicity, the model describes the structure initially closed in *y*-direction (figure 1(C)). Figure 3(A) presents the top views of

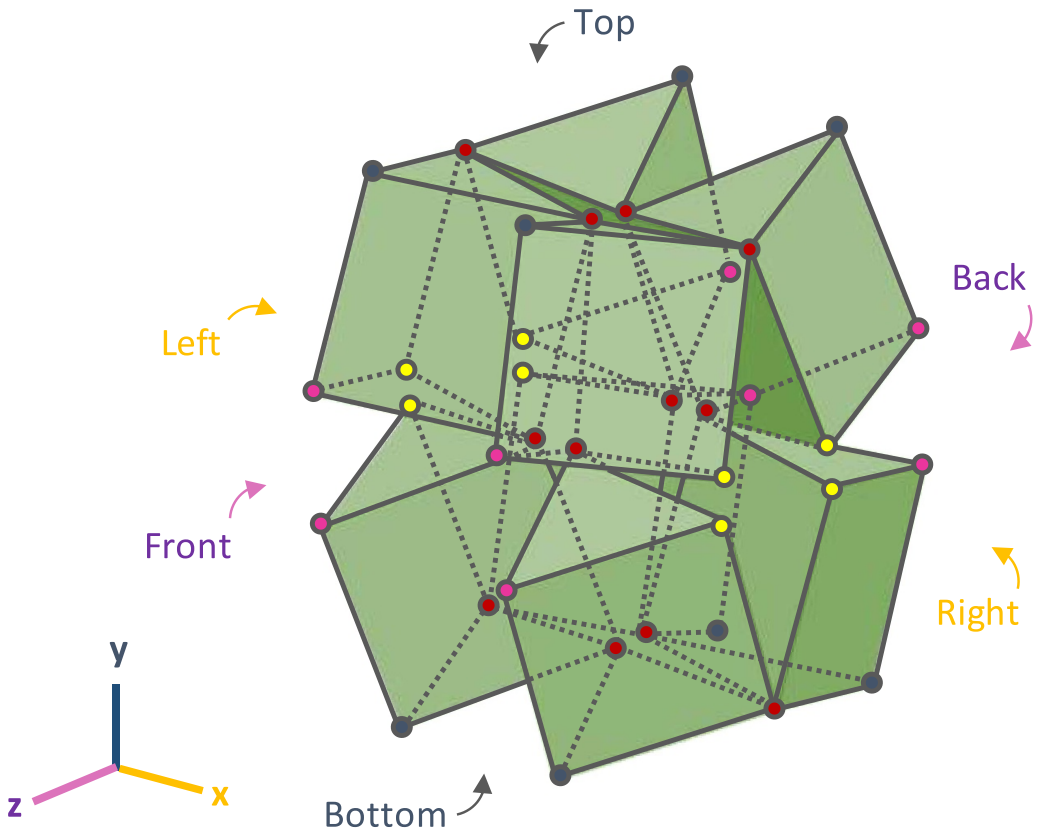

Figure 2. Edge vertices used for the implementation of periodic boundary conditions and hinged corners of the unit cell.

the metamaterial when fully compressed (i.e. when closed), corresponding to each value of the angle θ. Figure 3(B) shows three axonometric views of the corresponding closed configurations of the system (low, medium, and high level of the θ angle). The model applied a tensile displacement in y-direction to the structure along the vertices of the top and bottom surfaces of the metamaterial (white circles in figure 2). This corresponds to a 25% of the original height of the structure, with the exception of those metamaterial configurations in which the prisms come into contact during the deformation. Figure 3(C) shows the deformed (i.e. open) configuration of the metamaterial architecture with $\theta = 45°$ along the three principal planes of the system, where φ denotes the characteristic angle of the structure. By examining the displacement field predicted by the numerical model, we calculated the strains considering the variation of the distances between the paired vertices along the x, y and z-directions [39] denotes as P_R–P_L, Q_T–Q_B and R_F–R_B, respectively (figures 3(B) and (C)). Thus, from the computed strains, we calculated the Poisson's ratios of the metamaterial.

3.2. Design and AM of auxetic polyhedral metamaterials

This section focuses on the design and AM of the three configurations which, according to the kinematic analysis in section 3.1, exhibit the higher on-axis auxetic response (see section 4.1), and additionally, a characteristic angle, θ, that reduces the formation of sharp joints between the rotating polyhedrons. Specifically, we investigated the configurations with the internal angle θ equal to 30°, 45° and 60° (see figures 1 and 3), and the same open cell configuration as in the previous section (displacement in the y-direction equal to 25% of the original height, see figures 1(D) and 3(C)).

Specifically, we converted the ideal hinges connecting the solid polyhedrons in figure 4(A) into curvature-based ligaments at their vertices (figure 4(B)), thus introducing a geometric chiral characteristic in the metamaterial [53]. As shown in figure 4(B), these ligaments have a non-uniform thickness obtained from a combination of 3D variable circular arc fillets at the joint regions of the system [54, 55], which prevent localized stress concentration phenomena. Considering that auxeticity is a scale-independent property, we set the height of the triangular prims of the RUC, h, equal to 5 mm and considered an aspect ratio (h/l) equal to 1 (see figure 1). As a result, the minimum ligament thickness in the system, i.e. t, was set equal to 1.5 mm (figure 4(B)), which allow to fabricate self-supported ligaments between the prism thus avoiding undesirable defects on the system. Additionally, we fillet the edges of each polyhedron, resulting in a structure with smooth rigid units which are easy to manufacture. Figure 5(B) presents the top views of the corresponding open RUC designs with ligaments, namely as *Architecture I, Architecture II* and *Architecture III*, where θ' indicates the internal angle of the designed metamaterial architectures, whose values are equal to 7°, 21° and 38°

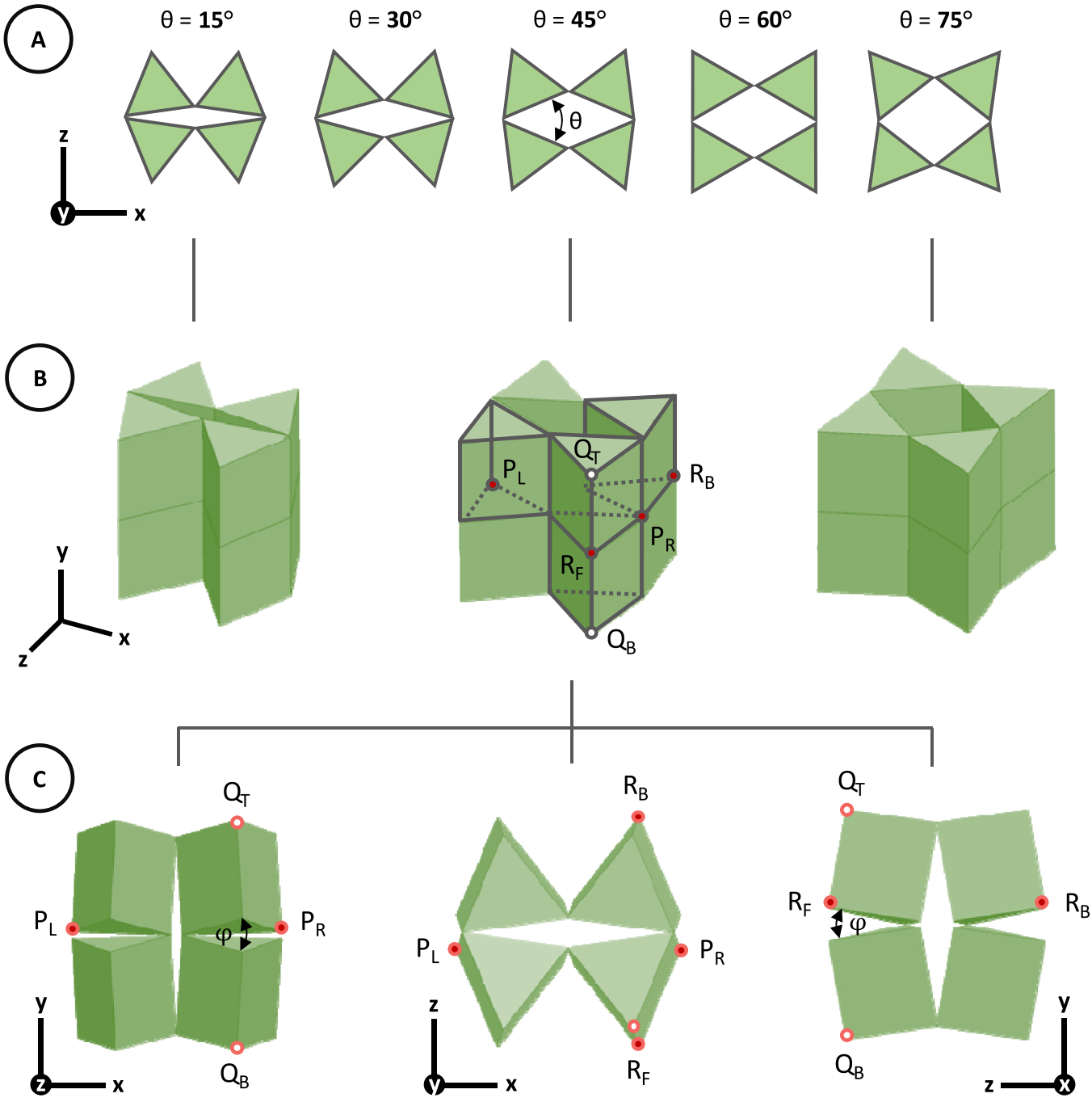

Figure 3. Top views of the three-dimensional metamaterial (A) in their undeformed (i.e. closed) configurations. Axonometric views of three corresponding closed configurations of the system (B). Deformed (i.e. open) configuration of the metamaterial ($\theta = 45^\circ$) along the three principal planes of the structure (C).

respectively. Moreover, as depicted in figure 5(B), all the designed architectures present the same value of the characteristic angle, denoted by φ, which was set equal to 35°.

Using AM technology, we manufactured a specimen for each of these architectures, including 2×2 × 2 RUC of the metamaterial (figure 5(C)). The designed configurations were built on a fused filament fabrication *Markforged* 3D printing machine using a micro carbon fiber filled polyamide (*Onyx*™) material and optimized parameters to ensure high quality prototypes. Specifically, we considered a 35% infill density with a hexagonal pattern and used a layer thickness equal to 0.2 mm. In order to avoid any supports during printing, the prototypes were printed along the transversal z-direction (see figure 5(A)). The specimens have relative density ranging from 27% to 30%, with a minimum transversal dimension of 71 mm for the *Architecture I* and a maximum length of 75 mm corresponding to the *Architecture III*, where the height of prototypes in y-direction is equal to 80 mm.

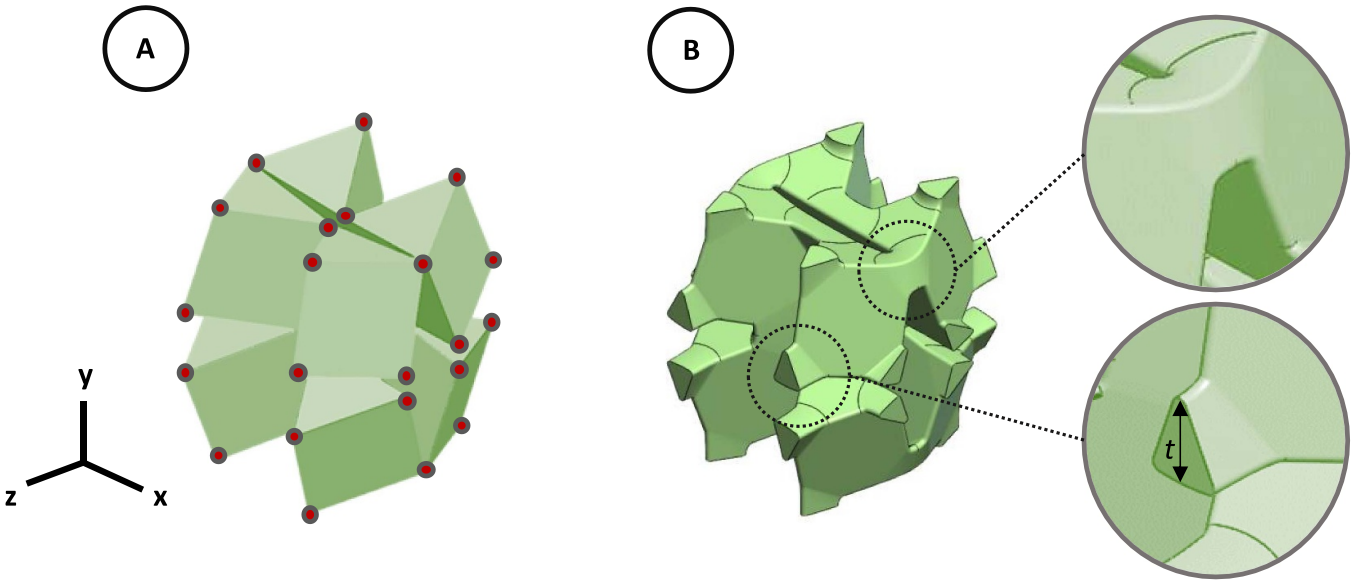

Figure 4. Open cell configuration of the metamaterial: (A) idealized hinged structure and (B) designed unit cell motif with ligaments at the joint regions of the system.

3.3. Experimental validation

In order to evaluate the *quasi-static* mechanical properties of the three metamaterial configurations described in the previous section, the AM-ed prototypes were tested under uniaxial compression using a *Galdabini SUN 500* electromechanical testing machine with a 5 kN load cell. The *quasi-static* tests were conducted at a rate of 1 mm min^{-1}, up to a final displacement in y-direction equal to 2.4 mm, which corresponds to an overall global strain of the sample equal to 3%; this allows to limit the value of stresses in the joint regions of the system below the ultimate compressive stress of the *Onyx* material (for details see section 3.4) [35]. The data associated to the load and to the displacement were acquired and used to elaborate the stress–strain curve of the metamaterials. Hence, the Young's modulus of the systems, E_y, was calculated from the linear region of the resulting stress–strain curves, according to the standards [56].

During the compression tests, we measured the displacement field of the samples at three levels of the applied global strain, corresponding to 1%, 2% and 3% of the initial height of the prototypes. Since the deformation behavior of the samples was affected by the boundary conditions, the displacement field of the system was measured on the central RUC of the two longitudinal planes of the structure (i.e. plane yx and plane yz in figure 6) by using two independent varifocal digital cameras. Then, we calculated the strains of the structure trough image post-processing in *Matlab* environment [57], by tracking the centroids of voids surrounding the central RUC of the samples (i.e. the red dots in figure 6) [58, 59]. Thus, we calculated the average centroid-to-centroid distances during the deformation along the three directions, namely $\overline{\delta}_x$, $\overline{\delta}_y$ and $\overline{\delta}_z$, and obtained the average strains as

$$\bar{\varepsilon}_{xx} = \frac{\overline{\delta}_x}{L_x}, \qquad \bar{\varepsilon}_{yy} = \frac{\overline{\delta}_y}{L_y}, \qquad \bar{\varepsilon}_{zz} = \frac{\overline{\delta}_z}{L_z}, \tag{1}$$

where L_x, L_y and L_z represent the initial distances between the centroids along the x, y and z-direction in the undeformed configuration respectively. Then, the local average Poisson's ratios are given by

$$\nu_{yx} = -\frac{\bar{\varepsilon}_{xx}}{\bar{\varepsilon}_{yy}}, \qquad \nu_{yz} = -\frac{\bar{\varepsilon}_{zz}}{\bar{\varepsilon}_{yy}}. \tag{2}$$

3.4. Nonlinear FE analysis

For the three metamaterial configurations investigated experimentally in section 3.3, we also simulated the compression behavior of the polyhedral structures in figure 5 through 3D FE models using the implicit solver of *Abaqus* [60]. In particular, the nonlinear static simulations examined both equivalent periodic domains and finite-size of each architecture, where the latter reproduce the same models fabricated though AM techniques.

Specifically, for the case of the infinite systems, we considered only one-eight of the RUC under PBCs [35, 61], see figure 7(A). In order to implement the periodic symmetry of the rotating prism of the RUC, the model applied simple supports to the nodes at the bottom horizontal face, on the left vertical face and on the back vertical face, figure 7(A). On the remaining faces the model implemented a planar surface internal constraint. Specifically, on the front vertical face the

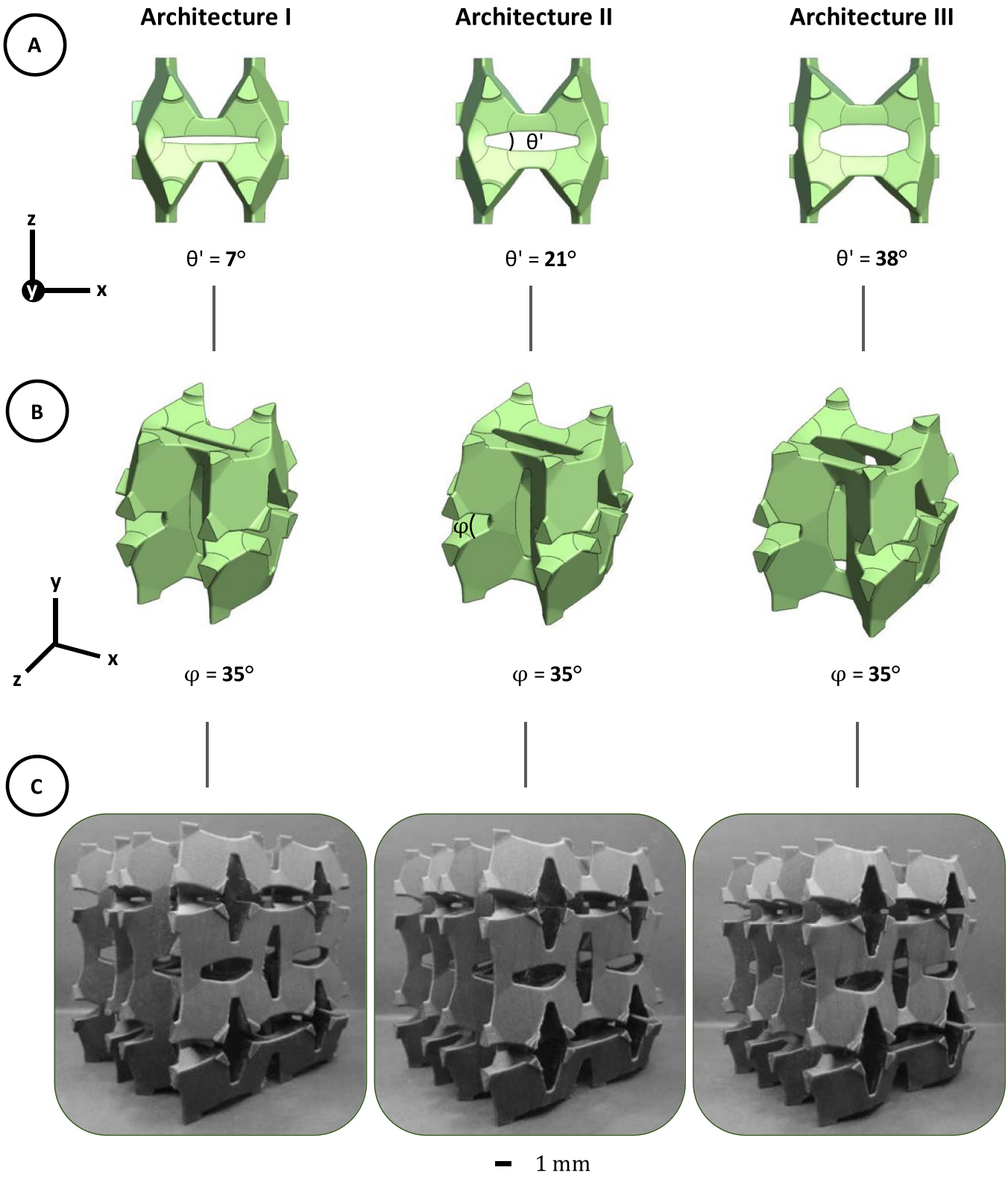

Figure 5. Design types: (A) top and (B) axonometric view of the designed RUCs. 3D printed prototypes of the metamaterial configurations investigated (C).

constraint makes equal the displacement of the nodes in the z-direction; similarly, on the right vertical face the constraint makes equal the displacement of the nodes in the x-direction. To reach the desired global strain, the model applies a vertical displacement on the top horizontal nodes, equivalent to a 3% of the height of the prism (see figure 7(A)).

On the other hand, for finite systems, the models were constrained in a similar way to that used in the experiments,

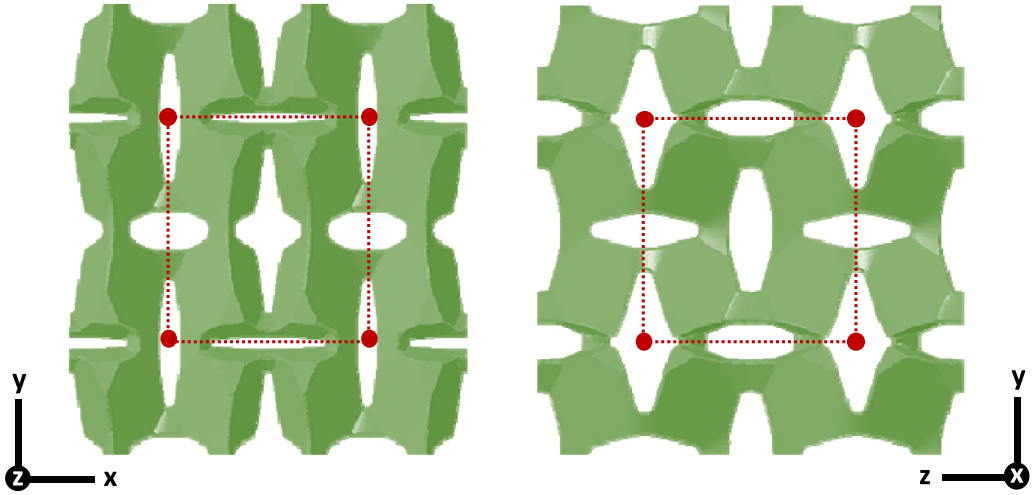

Figure 6. Centroids used for calculating the PRs along the *yx* and *yz* planes of the metamaterial.

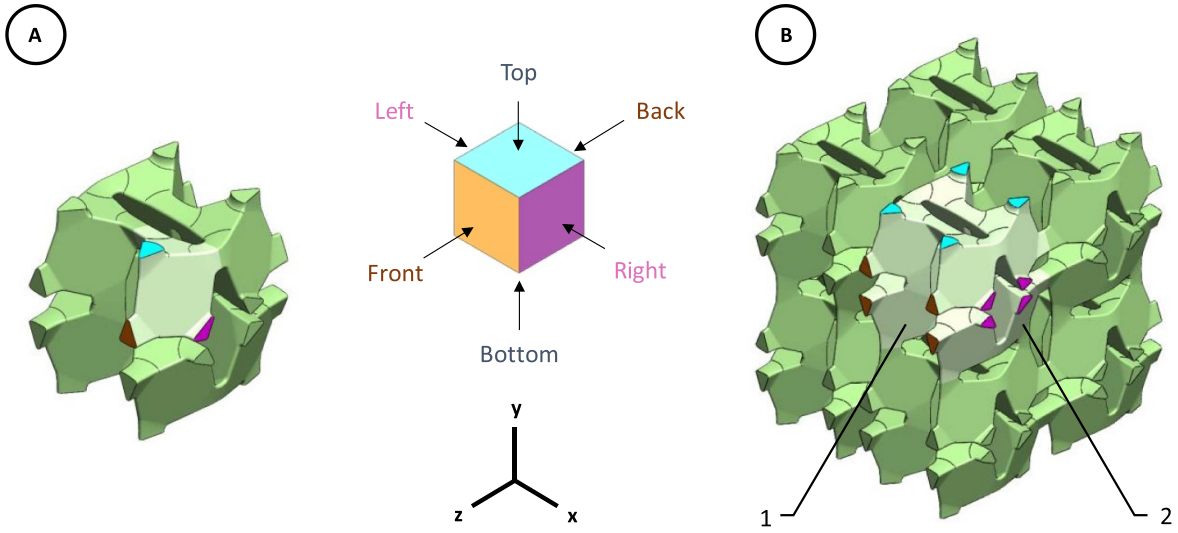

Figure 7. Equivalent periodic (A) and finite-size (B) domains of the simulated metamaterial with indication of face sets used to prescribe the boundary conditions.

assuming a frictionless contact between the prototypes and the plates of the testing machine (see section 3.3). Considering that the structures have three planes of symmetry aligned along each of the three main Cartesian planes (figure 5), the FE models implement a single RUC of the metamaterial and constrained the system by applying simple supports to the nodes at the bottom horizontal faces, on the back vertical faces and on the left vertical faces, figure 7(B). Hence, the right and front faces of the structure were left unconstrained. The model applies a compressive displacement on the top horizontal faces of the system up to a value of global strain identical to that one applied in the experimental tests, figure 7(B).

For all the simulated systems, we discretized the structure using second-order tetrahedral elements (C3D10 in *Abaqus* [60]). According to a mesh convergence analysis, the side length of the element was in the range between 0.1 mm, along the ligaments, and 0.15 mm in the rest of the model. The model describes the polymeric material using an isotropic elasto-plastic constitutive law: specifically, the material properties of Onyx come from uniaxial tensile tests on dog-bone specimens according to *ASTM D638* standard [62]. In particular, a Young's modulus, E_{m}, of 357 MPa and a Poisson's ratio, ν, of 0.34 were applied to the elastic model and a yield stress, $\sigma_{y,\mathrm{m}}$, of 12 MPa was used for the plasticity model.

Hence, the elastic modulus of the metamaterials, E_y, was calculated at the beginning of the linear region of the stress–strain curve. In addition, the FE model provided the Poisson's ratios (PRs) of the structures, namely ν_{yx} and ν_{yz}. On the one hand, for the case of infinite systems, the analyses evaluated the relative displacements of the ligaments of the simulated cell and compared them to the initial dimensions of the structure, thus obtaining the relative strains of the prism. On the other hand, for the case of finite-size simulations, the analyses calculated the displacements of the ligaments surrounding the central rotating unit along the two transverse planes of the metamaterial (denoted as *1* and *2* in figure 7(B)), which are

used to derive the local axial and transverse strain values. Thus, for both the numerical models, the derived strain values were used to calculated the local Poisson's ratios of the metamaterial architectures (for further details see [63]). Finally, the analysis provided the equivalent plastic strain in the metamaterial.

4. Results and discussion

4.1. Kinematic model results

Figure 8 shows the auxetic behavior of three configurations of the hinged structure for different values of the characteristic angle, θ, along the principal planes of the system, where the aspect ratio, h/l, was kept constant to 1 (see section 2). As emerges from figure 8, all the simulated architectures exhibit a significantly NPR property in all principal directions. This results from the tilting of the prisms at their vertices that originates void spaces in the structure, and thus an increase of the apparent volume of the metamaterial. In particular, the rigid units rotate around their internal pivots (i.e. the corners), and therefore, rotate towards the center of the structure while expand in transverse direction in response to a tensile strain in the y-direction, confirming the auxetic potential of the proposed architecture. However, viewing the structure in the xz plane, i.e. the left column in figure 8, the tilt in x- and y-direction is predominant with respect to the third direction considered (z-direction).

Moreover, the metamaterial configuration in figure 8(A) experienced a maximum tensile strain of 15%, since the internal edges of the polyhedrons come into contact during the deformation due to the low value of the angle θ. Conversely, for high value of θ, the polyhedrons are freely to rotate even for high value of axial strain (figures 8(B) and (C)), also for the case of θ equal to 75°, where the expansion of metamaterial in x-direction is limited to the increasing of the internal angle of the system. This confirms the assumption of the limit of the angle θ in the kinematic model described in section 3.1. Furthermore, the range of the internal angle, θ, showing NPR behavior can be increased by connecting the rotating units with chiral ligaments or by increasing the characteristic angle of the metamaterial, namely φ, up to axial strains below 25% of the system (see figure 1). Animations showing the kinematic behavior of the architected materials in figure 8 are presented in the supplementary material.

Figure 9 presents the variation of PR of the metamaterial in all the principal directions, as a function of the internal angle θ and of characteristic angle φ (see figure 1). The results in figure 9 highlight that the system possesses anisotropic NPRs, whose values are nearly constant over the strain range considered, where the maximum variation was about 3%. This behavior over classes the results obtained from previous studies on auxetic rotating unit architectures, such as in the case of regularly configured structures with polygonal prisms [41]. By focusing on the value of the characteristic angle, namely φ, it reaches a maximum of 40° for $\theta = 75°$ and $h/l = 1$, while becomes equal to 12° for $\theta = 15°$ and $h/l = 1.5$ (see figure 9).

Careful examination of figure 9 indicates that, for $h/l = 1$, by increasing the value of the internal angle, θ, the values of ν_{xy}, ν_{xz} and ν_{zy} increase (figures 9(A), (C) and (E)), with the only exception for the architecture with θ equal to 75°, showing a more negative value of ν_{zy}. Hence, the increase of φ, causes a slightly decrease of the PRs even for constant value of the angle θ. In more detail, for θ equal to 15° and $h/l = 1$, ν_{xy} attains to a minimum value of -2.79, corresponding to a maximum value of ν_{yx} equal to -0.27. In addition, the increase of the ratio h/l, causes an increase of the values of ν_{xy}, ν_{xz} and ν_{zy} whit a similar trend to that observed for the architectures with $h/l = 1$. On the other hand, considering the ratio h/l equal to 1, the value of ν_{yx} and ν_{zx} significantly increase to negative values if θ increases (on the right of figures 9(B) and (D)). Thus, ν_{yz} decreases by increasing the value of θ up to 60°: over this point, it starts to increase, see figure 9(F). Conversely, when the value of h/l increases, PRs denoted as ν_{yx}, ν_{zx} and ν_{yz} become more negative, with a minimum of -3.55 for the case of $\theta = 75°$. In conclusion, the results in figure 9, prove that, with the exception of the φ angle, the geometric parameters of the polyhedrons have an enormous effect on auxeticity of the metamaterial, depending on the angle θ. Hence, since the hinges at the vertices of the polyhedrons were assumed as ideal, the NPR of the system were found to depend only on the shape of the prisms and on the direction of the loading. From this investigation emerges that the most promising architectures in terms of auxetic response and geometrical characteristics are the ones with $\theta = 30°$, 45° and 60°.

4.2. Experimental results and FE simulations

Figure 10 shows the undeformed and the deformed system configurations obtained experimentally of the three AM-ed chiral architectures investigated in section 3.2, and corresponding to an angle θ equal to 30°, 45° and 60°. These refer to the deformation behavior of the metamaterial designs along the frontal plane of the structure, namely the xy plane. All the designs in figure 10 exhibit a NPR as highlighted by the reduction of the apparent volume of the structures: specifically, the elliptical voids surrounding the central unit of the metamaterials (colored profiles in figure 10) exhibit a reduction of their minor axis as a consequence of the axial compression, which can be primarily attributed by the rotation of the semi-rigid polyhedrons. This effect testified the auxeticity of the metamaterial. Moreover, in their compressed configuration, the voids surrounding the central unit of the metamaterials retain their elliptical shape, which is very similar for all the architectures investigated. This phenomenon is plainly visible in the *Architecture III*, since it is characterized by the larger value of θ' (for details see figure 5). As clearly visible in figure 10, the larger the internal angle, θ', of the designed architectures, ranging from 7° for the *Architecture I*, to 38° for the *Architecture III*, the higher the auxetic behavior of the structure. This auxetic response comes from the peculiar configuration of the ligaments that connect the rotating polyhedrons: since the ligaments bend whilst the rigid units rotate, the architectures have a NPR characteristic as observed in the polyhedral mechanism with ideal hinges at their vertices (see section 4.1).

FE predictions of the deformation mechanism of the RUC of each architecture are also reported in figure 11(A),

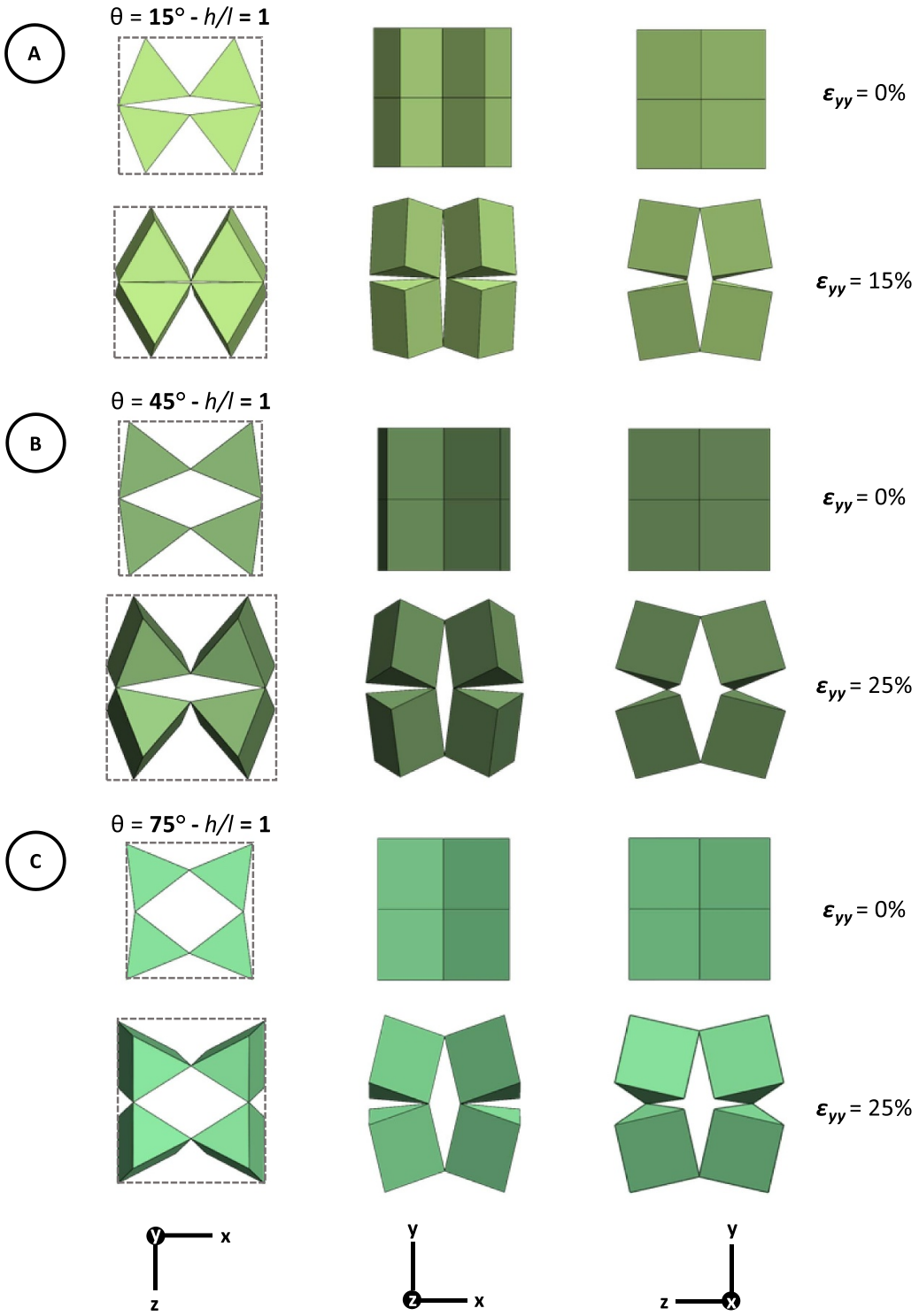

Figure 8. Kinematic model results: undeformed and deformed configurations of the metamaterial with low (A), medium (B) and high (C) value of angle θ along the principal planes of the structure, where the ratio h/l was kept constant to 1 (see section 2). The change in linear dimensions of the metamaterial configurations along the transverse directions of the structure was highlighted by the dashed lines in the first column in the figure.

according to the model described in section 3.4. In accordance with the experimental observations (figure 10), these results confirm the auxetic response of the chiral polyhedrons with a reduction of the elliptical domains of the voids of the system on both their transverse planes.

Additionally, figure 11(B) shows the numerical prediction of the equivalent plastic strain distribution in the metamaterial designs, evaluated for a global axial strain equal to 3%. As evident from figure 11(B), the location of the plastic deformation was very similar for the three architectures,

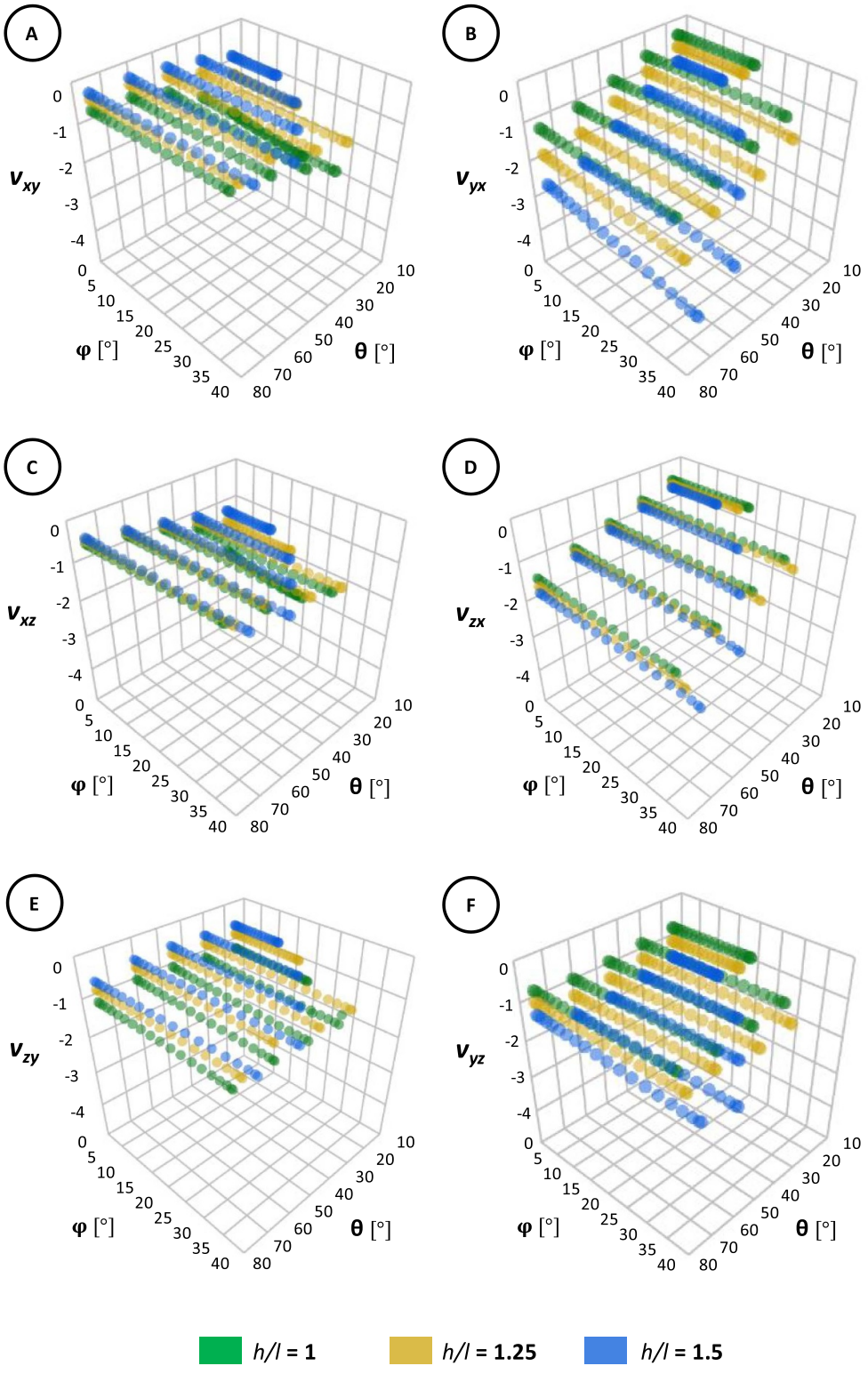

Figure 9. Evolution of Poisson's ratios of the hinged structure with variation in internal angle, θ, and characteristic angle, φ, upon the main Cartesian planes of the system: i.e. plane xy (A), (B), plane xz (C), (D) and plane zy (E), (F). For details on geometrical parameters of the structure see section 2.

regardless of the different internal angle of the polyhedrons, θ' (figure 5). Specifically, the structures exhibit high strain at the joint regions of the systems, especially along the vertical ligaments which experienced mainly compressive and bending strains, while the central units remain completely undeformed. This trend is typical of metamaterial architectures with chiral

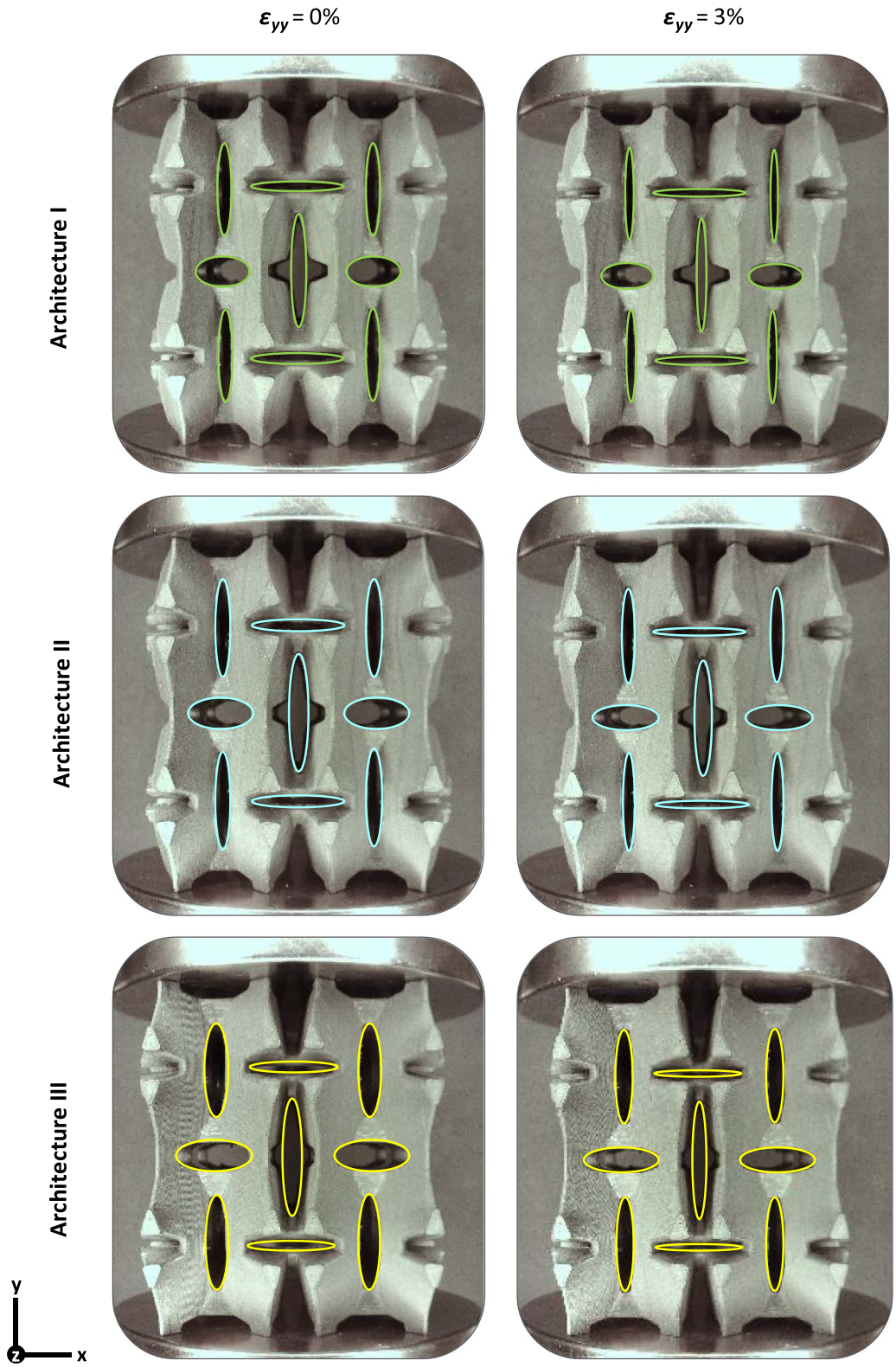

Figure 10. Undeformed and deformed system configurations of the AM-ed chiral architectures under uniaxial compression with highlighted variation of voids surrounding the central unit cell of the metamaterial along the *xy* plane of the system. For details see section 3.2.

characteristic retrieved from literature [64]. Specifically, the contour maps highlight a slight increase in the maximum plastic strain values by increasing the internal angle of the polyhedrons, with a peak of nearly 9% in the *Architecture III*. As suggested in the literature [35, 53], this strain value could be reduced by optimizing by the relative dimensions of the chiral ligaments compared to dimension of the central prisms. However, investigations of optimal stress/strain

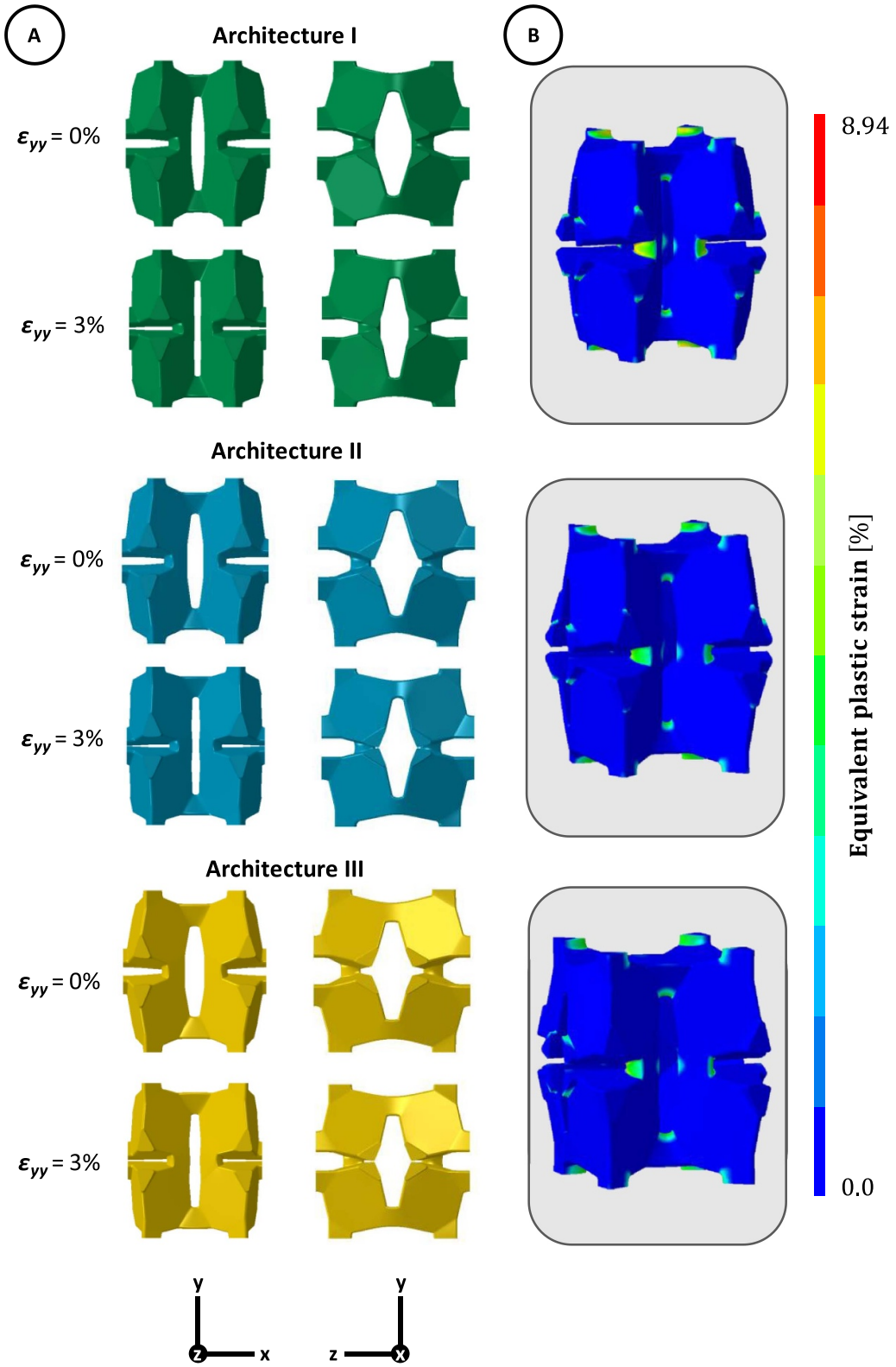

Figure 11. FE prediction of the undeformed and deformed chiral polyhedral architectures under uniaxial compression (A), see section 3.2. Equivalent plastic strain contour for a global strain of the structure equal to 3% (B).

design of the metamaterial were beyond the scope of this work.

In order to confirm these observations, figure 12 compares the computational and experimental Poisson's ratios of the polyhedral designs, where numerical models refer to both equivalent periodic domains (i.e. the prism) and finite-size (i.e. the RUC) of each metamaterial configuration (see section 3.4). As we expected, all the investigated

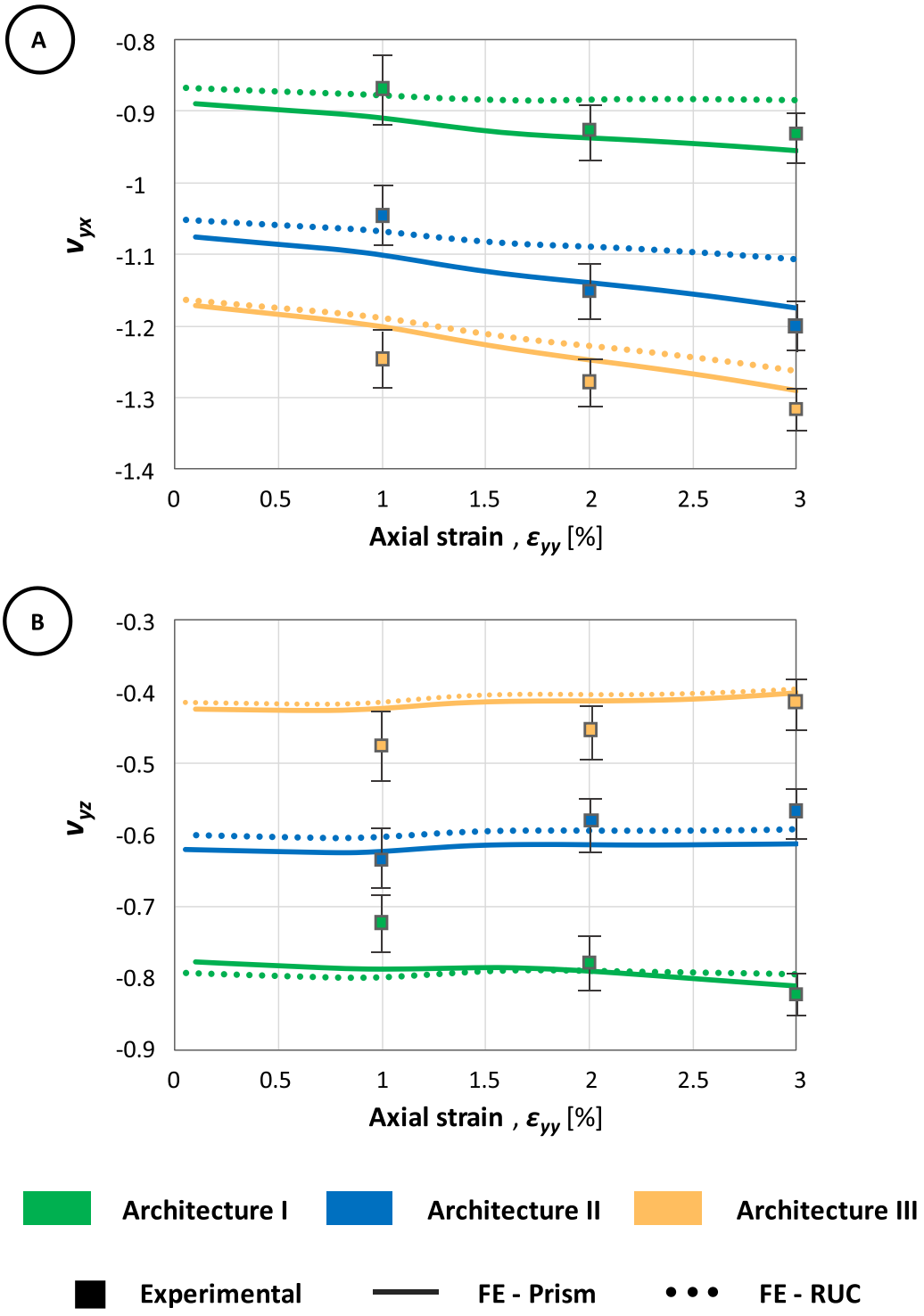

Figure 12. Comparison between the numerical and experimental on-axis Poisson's ratios of the three chiral architectures as a function of the axial strain: (A) v_{yx} and (B) v_{yz}, Experimental results reported the averaged Poisson's ratios, where the error bars were obtained from the standard deviation of the experimental PRs used in the averaging (see section 3.3).

architectures possess highly negative value of Poisson's ratio, showing an excellent quantitative agreement between experimental tests and numerical simulations, as well by comparing the results obtained from the different FE models. However, the values of v_{yx} slightly decrease over the range of axial strain (figure 12(A)), while v_{yz} is approximately constant for all the designs (figure 12(A)). Interestingly, we obtained a value of v_{yx} -0.9 for type *I* architecture, while becomes nearly equal to -1.3 for type *III* architecture. On the other hand, the value of v_{yz} steeply decreases to -0.4 for the *Architecture III*, while remains relatively unchanged for the *Architecture I*. The results in figure 12 highlights that, the values of Poisson's ratios in the metamaterial, were affected by the specific value of the internal angle between

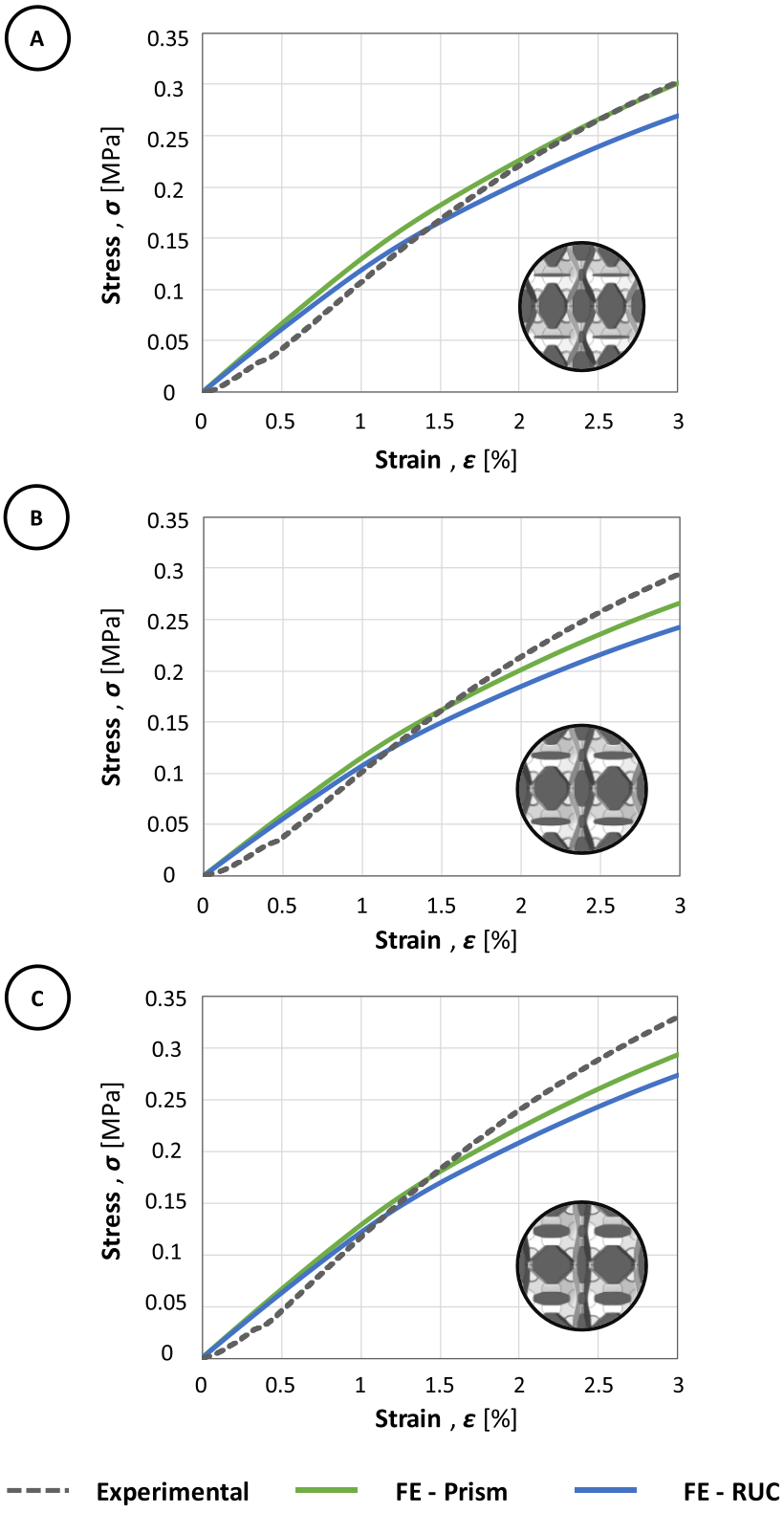

Figure 13. Comparison between the experimental and numerical stress–strain curves of the chiral designs investigated up to 3% overall strain: (A) *Architecture I*, (B) *Architecture II* and (C) *Architecture III*. For details on numerical models see section 3.4.

the polyhedrons (i.e. θ' in figure 5). This trend is congruent with findings from similar structures with 3D rotating prisms [35, 41]. Moreover, these results demonstrate that, the auxetic polyhedral structure outperform most of the 3D chiral and the re-entrant structures proposed in the literature in terms of NPR [7].

Figure 13 reports the stress–strain curves of the metamaterial architectures by comparing the experimental results

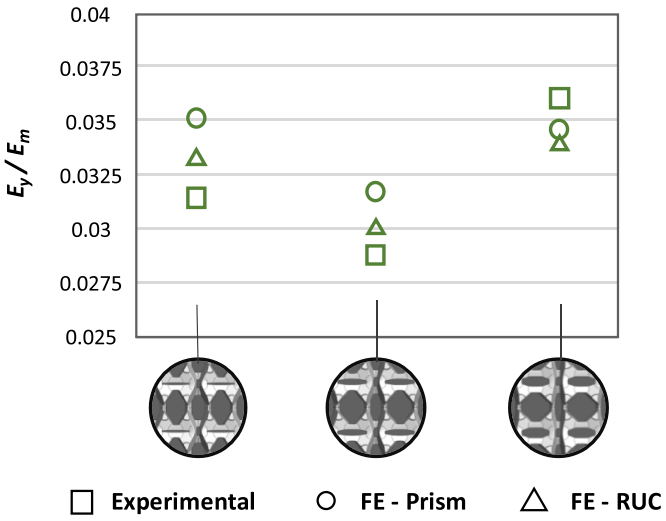

Figure 14. Normalized elastic modulus, E_y/E_m, of *Architecture I* (left), *Architecture II* (central) and *Architecture III* (right).

with those obtained from computational predictions (see sections 3.3 and 3.4). From figure 13, it is evident that all the material designs showed a similar behavior over the applied strain, exhibiting a good agreement between experimental and numerical results. Specifically, the curves were characterized by an initial linear elastic region, with a very similar trend for the *Architecture I* and *Architecture II* (figures 13(A) and (B)), and followed by a gradual increase in the stress, which is predominant in the *Architecture III* in figure 13(C).

On one hand, with regard to numerical results in figure 13, it could be noticed that the mechanical response of the metamaterial within the elastic region is nearly the same for both FE models, regardless they describe a single RUC or the whole specimen, and regardless of the prescribed boundary conditions [65]. In addition, the elastic region of the metamaterial is independent of the orientation of the auxetic polyhedrons, i.e. of the internal angle, θ' (figure 5). From a 1.5% value of the engineering strain, the numerical stress–strain curves diverge from the experimental curve (dashed curve in figure 13). On the other hand, the experimental tests exhibit a higher stiffness and nearly linear response of the metamaterial compared to the prediction from the computational models. The differences between the numerical prediction and experimental response can be primarily attributed to the following issues. First, the difference in the boundary conditions between the tests and the simulations, especially for the case of finite-size models. Second, the differences between the ideal geometry of the numerical model and the real geometry of the specimen featuring geometrical imperfections typical of 3D printing. Third, the large variance in the mechanical properties of the 3D printed material.

Figure 14 presents a synthesis of the normalized elastic modulus (i.e. Young's modulus) of the metamaterial configurations. From figure 14 emerges that, the value of the normalized elastic modulus of the structure is nearly the same for the three architectures, assuming a value in the range between 2.8% and 3.6%. By comparing the experimental measurements with FE prediction it appears a good agreement, specifically for *Architecture I*, with a 5% difference. These findings indicate that the value of relative Young's modulus of this system is about two order of magnitude higher than the one of the chiral-rotating motif proposed by the same authors [35].

By comparing the results obtained from the kinematic models on hinged structure systems (figures 8 and 9), with those obtained for the real geometries that replace the hinge with a ligament (figures 10 and 12) it appears a significant difference in the PR of the metamaterial: this is a direct consequence of the chiral characteristic due to the ligament between the prisms, which causes a reduction of the auxetiticy of the system. The proposed solution has a number of possible applications, from meta-biomaterials, to the design of bone substitutes, in life-lasting orthopedic applications [66], where the elastic modulus of the titanium alloy (Ti6Al4V ELI) is generally higher than 90 MPa [67].

5. Conclusion

The present work proposed, designed and validated a new type of architected structure made of rotating triangular prisms connected by their vertices, that behaves as an auxetic solid. Specifically, we investigated the NPR property of the proposed polyhedral metamaterial through the implementation of kinematic models of the system and analyzed the effect of geometrical parameters of the prims on deformation behavior of the structure. From kinematic results, we identified a peculiar polyhedral cell configuration that features large values of NPR in all directions, up to -3.55. This configuration of the metamaterial was designed and AM-ed for three different values of the opening angle between the prisms by introducing ligaments to join the rotating prisms. These three designs were tested up to a 3% global compressive strain, showing anisotropic behavior and values of Poisson's ratio ranging between -0.4 up to -1.2. Two different FE models of this innovative metamaterial were then calibrated against the results of the experimental tests. Thanks to its peculiar mechanical response, this novel 3D auxetic metamaterial, can be used for biomechanical applications such as prostheses and provides a new paradigm for the design of 3D rotating architectures with others negative mechanical properties, such as negative compressibility and negative thermal expansion properties.

Data availability statement

The data that support the findings of this study are available upon reasonable request from the authors.

Funding

The author(s) received no financial support for the research, authorship, and/or publication of this article.

Conflict of interest

The author(s) declared no potential conflicts of interest with respect to the research, authorship, and/or publication of this article.

Credit statement

Andrea Sorrentino—Conceptualization, Methodology, Investigations, Formal Analysis, Writing—Original Draft. Davide Castagnetti—Conceptualization, Methodology, Formal Analysis, Writing—Review & Editing.

ORCID iDs

A Sorrentino https://orcid.org/0000-0002-7145-5219
D Castagnetti https://orcid.org/0000-0003-3300-5716

References

[1] Benedetti M, du Plessis A, Ritchie R O, Dallago M, Razavi S M J and Berto F 2021 Architected cellular materials: a review on their mechanical properties towards fatigue-tolerant design and fabrication *Mater. Sci. Eng.* R **144** 100606
[2] Surjadi J U, Gao L, Du H, Li X, Xiong X, Fang N X and Lu Y 2019 Mechanical metamaterials and their engineering applications *Adv. Eng. Mater.* **21** 1800864
[3] Zadpoor A A 2016 Mechanical meta-materials *Mater. Horiz.* **3** 371–81
[4] Berger J B, Wadley H N G and McMeeking R M 2017 Mechanical metamaterials at the theoretical limit of isotropic elastic stiffness *Nature* **543** 533–7
[5] Yu X *et al* 2018 Mechanical metamaterials associated with stiffness, rigidity and compressibility: a brief review *Prog. Mater. Sci.* **94** 114–73
[6] Ren X, Das R, Tran P, Ngo T D and Xie Y M 2018 Auxetic metamaterials and structures: a review *Smart Mater. Struct.* **27** 023001
[7] Kolken H M A and Zadpoor A A 2017 Auxetic mechanical metamaterials *RSC Adv.* **7** 5111–29
[8] Lakes R S 2017 Negative-Poisson's-ratio materials: auxetic solids *Annu. Rev. Mater. Res.* **47** 63–81
[9] Lakes R 1987 Foam structures with a negative Poisson's ratio *Science* **235** 1038–40
[10] Evans K E, Nkansah M A, Hutchinson I J and Rogers S C 1991 Molecular network design *Nature* **353** 124
[11] Grima J N, Caruana-Gauci R, Dudek M R, Wojciechowski K W and Gatt R 2013 Smart metamaterials with tunable auxetic and other properties *Smart Mater. Struct.* **22** 084016
[12] Evans K E and Alderson A 2000 Auxetic materials: functional materials and structures from lateral thinking *Adv. Mater.* **12** 617–28
[13] Choi J B and Lakes R S 1992 Non-linear properties of metallic cellular materials with a negative Poisson's ratio *J. Mater. Sci.* **27** 5375–81
[14] Argatov I I, Guinovart-Díaz R and Sabina F J 2012 On local indentation and impact compliance of isotropic auxetic materials from the continuum mechanics viewpoint *Int. J. Eng. Sci.* **54** 42–57
[15] Scarpa F *et al* 2006 Dynamic behavior and damping capacity of auxetic foam pads *Smart Structures and Materials 2006: Damping and Isolation* vol 6169 p 61690T
[16] Scarpa F, Ciffo L G and Yates J R 2004 Dynamic properties of high structural integrity auxetic open cell foam *Smart Mater. Struct.* **13** 49–56
[17] Evans K E 1991 Auxetic polymers: a new range of materials *Endeavour* **15** 170–4
[18] Wang Z, Luan C, Liao G, Liu J, Yao X and Fu J 2020 Progress in auxetic mechanical metamaterials: structures, characteristics, manufacturing methods, and applications *Adv. Eng. Mater.* **22** 1–23
[19] Lvov V A, Senatov F S, Veveris A A, Skrybykina V A and Díaz Lantada A 2022 Auxetic metamaterials for biomedical devices: current situation, main challenges, and research trends *Materials* **15** 1–26
[20] Wallbanks M, Khan M F, Bodaghi M, Triantaphyllou A and Serjouei A 2022 On the design workflow of auxetic metamaterials for structural applications *Smart Mater. Struct.* **31** 023002
[21] Lim T-C 2020 *Mechanics of Metamaterials with Negative Parameters* Engineering Materials (Singapore: Springer) (https://doi.org/10.1007/978-981-15-6446-8)
[22] Hu H, Zhang M and Liu Y 2019 *Auxetic Textiles* (Amsterdam: Elsevier) (https://doi.org/10.1016/C2016-0-04399-1)
[23] Lim T-C 2015 *Auxetic Materials and Structures* (Singapore: Springer) (https://doi.org/10.1007/978-981-287-275-3)
[24] Kelkar P U, Kim H S, Cho K-H, Kwak J Y, Kang C-Y and Song H-C 2020 Cellular auxetic structures for mechanical metamaterials: a review *Sensors* **20** 1–26
[25] Bertoldi K, Vitelli V, Christensen J and van Hecke M 2017 Flexible mechanical metamaterials *Nat. Rev. Mater.* **2**
[26] Wojciechowski K W, Alderson A, Grima J N and Scarpa F 2020 Auxetics and other systems with "negative" characteristics *Phys. Status Solidi* b **257** 1–4
[27] Askari M *et al* 2020 Additive manufacturing of metamaterials: a review *Addit. Manuf.* **36** 101562
[28] Wu W, Hu W, Qian G, Liao H, Xu X and Berto F 2019 Mechanical design and multifunctional applications of chiral mechanical metamaterials: a review *Mater. Des.* **180** 107950
[29] Grima J N, Alderson A and Evans K E 2005 Auxetic behaviour from rotating rigid units *Phys. Status Solidi* b **242** 561–75
[30] Grima-Cornish J N, Attard D, Grima J N and Evans K E 2022 Auxetic behavior and other negative thermomechanical properties from rotating rigid units *Phys. Status Solidi* **16** 1–24
[31] Grima J N and Evans K E 2000 Auxetic behavior from rotating squares *J. Mater. Sci. Lett.* **19** 1563–5
[32] Attard D, Manicaro E and Grima J N 2009 On rotating rigid parallelograms and their potential for exhibiting auxetic behaviour *Phys. Status Solidi* b **246** 2033–44
[33] Grima J N, Gatt R, Alderson A and E. Evans K 2005 On the auxetic properties of 'rotating rectangles' with different connectivity *J. Phys. Soc. Japan* **74** 2866–7
[34] Grima J N and Evans K E 2006 Auxetic behavior from rotating triangles *J. Mater. Sci.* **41** 3193–6
[35] Sorrentino A and Castagnetti D 2021 Negative Poisson's ratio lattice for designing vertebral biomaterials *Mechan. Adv. Mater. Struct.* **29** 6626–33
[36] Mizzi L *et al* 2021 A comparison between rotating squares and anti-tetrachiral systems: influence of ligaments on the multi-axial mechanical response *Proc. Inst. Mech. Eng.* C **235**
[37] Evans K E and Alderson A 2001 Rotation and dilation deformation mechanisms for auxetic behaviour in the α-cristobalite tetrahedral framework structure *Phys. Chem. Miner.* **28** 711–8
[38] Attard D and Grima J 2012 A three-dimensional rotating rigid units network exhibiting negative Poisson's ratios *Phys. Status Solidi* b **249** 1330–8

[39] Rueger Z, Ha C S and Lakes R S 2019 Flexible cube tilt lattice with anisotropic cosserat effects and negative Poisson's ratio *Phys. Status Solidi* b **256** 1–6
[40] Andrade C, Ha C S and Lakes R S 2018 Extreme Cosserat elastic cube structure with large magnitude of negative Poisson's ratio *J. Mech. Mater. Struct.* **13** 93–101
[41] Kim J *et al* 2017 Structures with polygonal prisms for three-dimensional auxetic behaviour *Proc. R. Soc.* A **473**
[42] Dagdelen J, Montoya J, De Jong M and Persson K 2017 Computational prediction of new auxetic materials *Nat. Commun.* **8** 1–8
[43] Tanaka H, Asao S and Shibutani Y 2021 Auxetic vibration behaviours of periodic tetrahedral units with a shared edge *R. Soc. Open Sci.* **8**
[44] Borcea C and Streinu I 2015 Geometric auxetics subject areas *Proc. R. Soc.* A **471**
[45] Kizilörenli E and Maden F 2021 Tessellation in architecture from past to present *IOP Conf. Ser.: Mater. Sci. Eng.* **1203** 032062
[46] Dragoni E and Ciace V A 2019 Mechanical design and modelling of lightweight additively manufactured lattice structures evolved from regular three-dimensional tessellations *Proc. Inst. Mech. Eng.* C **235** 1759–73
[47] Ciace V A, Dragoni E and Grasselli L 2022 From three-dimensional tessellations to lightweight filling materials for additively manufactured structures: concept, simulation, and testing *Proc. Inst. Mech. Eng.* L **236** 489–512
[48] Dudek K K, Attard D, Caruana-Gauci R, Wojciechowski K W and Grima J N 2016 Unimode metamaterials exhibiting negative linear compressibility and negative thermal expansion *Smart Mater. Struct.* **25** 25009
[49] Dudek K K, Martínez J A I, Ulliac G and Kadic M 2022 Micro-scale auxetic hierarchical mechanical metamaterials for shape morphing *Adv. Mater.* **34** 2110115
[50] Lakes R 2019 *Composites and Metamaterials* (Singapore: World Scientific) (https://doi.org/10.1142/11715)
[51] Dassault Systèmes 2022 SolidWorks (available at: www.solidworks.com/it)
[52] Okereke M and Keates S 2018 *Boundary Conditions BT—Finite Element Applications: A Practical Guide to the FEM Process* ed M Okereke and S Keates (Cham: Springer) pp 243–97
[53] Sorrentino A, Castagnetti D, Mizzi L and Spaggiari A 2022 Bio-inspired auxetic mechanical metamaterials evolved from rotating squares unit *Mech. Mater.* **173** 104421
[54] Sorrentino A, Castagnetti D, Spaggiari A and Dragoni E 2019 Shape optimization of the fillet under a bolt's head *J. Strain Anal. Eng. Des.* **54** 247–53
[55] Sorrentino A , Castagnetti D, Mizzi L and Spaggiari A 2021 Rotating squares auxetic metamaterials with improved strain tolerance *Smart Materials and Structures* **30**
[56] ASTM International 1981 Standard test method for Young' s modulus, tangent modulus, and chord modulus E111-17 (available at: www.astm.org/cgi-bin/resolver.cgi?E111-17)
[57] MATLAB 2010 Version 7.10.0 (R2010a) (Natick, MA: The MathWorks Inc.)
[58] Bertoldi K, Reis P M, Willshaw S and Mullin T 2010 Negative Poisson's ratio behavior induced by an elastic instability *Adv. Mater.* **22** 361–6
[59] Babaee S, Shim J, Weaver J C, Chen E R, Patel N and Bertoldi K 2013 3D soft metamaterials with negative Poisson's ratio *Adv. Mater.* **25** 5044–9
[60] Smith M 2009 *ABAQUS/Standard User's Manual, Version 6.9* (Johnston, IL: Dassault Systèmes Simulia Corp)
[61] Mizzi L *et al* 2020 Implementation of periodic boundary conditions for loading of mechanical metamaterials and other complex geometric microstructures using finite element analysis *Eng. Comput.* **37** 1765–79
[62] American Society for Testing and Materials. ASTM D638-14 2016 Standard practice for preparation of metallographic specimens *ASTM Int.* **82** 1–15
[63] Omairey S L, Dunning P D and Sriramula S 2019 Development of an ABAQUS plugin tool for periodic RVE homogenisation *Eng. Comput.* **35** 567–77
[64] Mousanezhad D, Haghpanah B, Ghosh R, Hamouda A M, Nayeb-Hashemi H and Vaziri A 2016 Elastic properties of chiral, anti-chiral, and hierarchical honeycombs: a simple energy-based approach *Theor. Appl. Mech. Lett.* **6** 81–96
[65] Peng C, Tran P, Nguyen-Xuan H and Ferreira A J M 2020 Mechanical performance and fatigue life prediction of lattice structures: parametric computational approach *Compos. Struct.* **235** 111821
[66] Zadpoor A A 2020 Meta-biomaterials *Biomater. Sci.* **8** 18–38
[67] Shirzad M, Zolfagharian A, Bodaghi M and Nam S Y 2023 Auxetic metamaterials for bone-implanted medical devices: recent advances and new perspectives *Eur. J. Mech.* A **98** 104905